SINOGRAM IMAGE COMPLETION FOR LIMITED ANGLE TOMOGRAPHY WITH GENERATIVE ADVERSARIAL NETWORKS

Seunghwan Yoo[1]*, Xiaogang Yang*[2]*, Mark Wolfman*[2]*, Doga Gursoy*[1,2]*, and Aggelos K. Katsaggelos*[1]
[1]Dept. of Electrical Eng. and Computer Science, Northwestern University, Evanston, IL 60208, USA
[2]Advanced Photon Source, Argonne National Laboratory, Lemont, IL 60439, USA

ABSTRACT

In this paper, we present a novel approach based on deep neural network for solving the limited angle tomography problem. The limited angle views in tomography cause severe artifacts in the tomographic reconstruction. We use deep convolutional generative adversarial networks (DCGAN) to fill in the missing information in the sinogram domain. By using the continuity loss and the two-ends method, the image completion in the sinogram domain is done effectively, resulting in high quality reconstructions with fewer artifacts. The sinogram completion method can be applied to different problems such as ring artifact removal and truncated tomography problems.

***Index Terms*—** Limited angle tomography, sinogram image completion, deep convolutional generative adversarial networks

1. INTRODUCTION

In principle, tomography needs projections to be collected at a 180° range of tilt angles, but it is often not possible to obtain a full angle tomography due to the characteristics of the samples or the limitations of the mechanical system that holds the sample. Figure 1 illustrates the limited angle tomography (LAT) problem and the resulting artifacts from reconstruction. The sinogram of the full angle tomography for the Shepp-Logan phantom is shown in Fig. 1 (a), which is from 180 projections with angular increments of 1°. Figures 1 (b) and (c) show two LAT with missing angles (30°, 60°). The reconstructions from the LAT have streaks and elongation artifacts while that of the full angle tomography is almost the same as the original phantom image as shown in Figs. 1 (d-f). As the missing angle increases, the artifacts become more severe.

Different types of approaches have been developed to tackle the LAT. The artifacts from the LAT problem can be mitigated with post-processing. Filtering can be performed on the reconstruction to suppress the artifacts, such as, a low-pass, bilateral [1], and nonlinear anisotropic diffusion filtering [2], to name a few. Zhang *et al.* [3] proposed a convolutional neural network (CNN) to correct the artifacts by learning the end-to-end mapping between the filtered back-projection (FBP) reconstructed images with the artifacts and artifact-free images. Sparsity-based regularization has also been popular [4–7]. Frikel [4] used sparsity-based regularization with a curvelet to compensate for the missing information. Goris *et al.* [5] proposed to use sparsity in the gradient domain to reduce the artifacts by using total variation (TV) regularization. Other approaches [6, 7] proposed to use the anisotropic TV algorithm taking into account characteristics of the artifacts to efficiently suppress them.

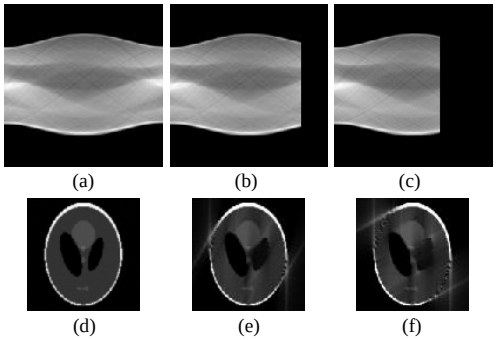

Fig. 1: (a, b, c) Sinograms of different angle projections with 180°, 150°, 120° of Shepp-Logan phantom, and (d, e, f) filtered back-projection reconstructions from the sinograms in (a, b, c)

Extrapolation-based approaches are also popular [8–10]. Such approaches directly fill in the missing data in the sinogram domain with the use of some constraints. Yau *et al.* [8] designed a linear extrapolator for limited angle sinograms based on sampling theory and regularization. Happonen and Ruotsalainen [9] presented the extrapolation of incomplete sinogram data in the sinogram and stackgram domains based on the Gerchberg–Papoulis algorithm [11]. Huang *et al.* [10] performed regression based on the Helgason-Ludwig consistency condition to fill in the missing area in the sinogram with image fusion in the frequency domain as post-processing.

The recent success of deep neural networks (DNNs) in image processing and computer vision boosted the performance of the image completion task [12–15], which can be applied to the image extrapolation problem. Van den Oord *et al.* [12] presented a DNN to sequentially predict the pixel values along the two spatial dimensions, showing that it can learn the local and long-range correlations. Pathak *et al.* [13] proposed a DNN to fill in the central square region of an image by using an encoder-decoder architecture to capture the context of an image. They used the adversarial loss to generate a perceptually natural scene. Gao and Grauman [14] suggested an on-demand learning algorithm to obtain a DNN that performs image inpainting with missing regions being at different locations and of different sizes. Yeh *et al.* [15] proposed an image completion method based on a deep convolutional generative adversarial network (DCGAN). Their loss function combines a contextual loss to preserve the given information and a perceptual loss to encourage the realistic look of the output image.

In this paper, we present a DCGAN-based extrapolation method to solve the LAT problem. Inspired by [15], we propose to use a

This research used resources of the Advanced Photon Source, U.S. Department of Energy (DOE) Office of Science User Facility operated for the DOE Office of Science by Argonne National Laboratory under Contract No. DE-AC02-06CH11357. M.W. acknowledges support by the DOE, Office of Science, Office of Workforce Development for Teachers and Scientists, Office of Science Graduate Student Research program under contract number DE-SC0014664. We acknowledge support through the NorthEast Center for Chemical Energy Storage, an Energy Frontier Research Center funded by the DOE, Office of Science, Basic Energy Sciences under Award DE-SC0012583 for materials and labor in development of the in-situ X-ray cell.

DCGAN for completing the missing angle data in the sinogram domain. We incorporate the continuity loss to make a smooth transition across the boundary, and use the two-ends method to improve the performance of image completion. We also show other applications of the proposed method to solve similar sinogram completion problems such as the ring artifact removal and truncated tomography problems. We describe the DCGAN for image completion in Section 2. The proposed algorithms for sinogram completion are introduced in Section 3. Experimental results and discussion are provided in Section 4 and we conclude our paper in Section 5.

2. DCGAN FOR IMAGE COMPLETION

2.1. DCGAN

GAN is a DNN-based generative model that is trained by two competing neural network models: a generator and a discriminator [16]. The deep convolutional GAN (DCGAN) introduces the CNN architecture into the GAN to generate image data more efficiently [17].

Let G and D denote the generative and discriminative networks of a DCGAN, respectively. Given a random vector, $\mathbf{z}$, with a distribution $p_{\mathbf{z}}$ as an input, G generates an image, $G(\mathbf{z})$. D maps an input image to the probability that the input is from the true data distribution, p_{data}. The output of D should be close to one if the input image is from p_{data}, and close to zero otherwise. While G tries to generate realistic images, D tries to distinguish images from p_{data} and those generated from G. The networks are trained by the minimax game, that is,

$$\min_G \max_D V(G,D) = \mathbb{E}_{\mathbf{x}\sim p_{data}(\mathbf{x})}[\log D(\mathbf{x})] + \mathbb{E}_{\mathbf{z}\sim p_{\mathbf{z}}(\mathbf{z})}[\log(1 - D(G(\mathbf{z})))], \quad (1)$$

where $\mathbf{x}$ is an image from p_{data}.

2.2. Image Completion with DCGAN

Once a DCGAN is trained to generate images in a certain domain, the trained G and D can be utilized to perform image completion [15]. Given a corrupted image, $\mathbf{y}$, the mask of the known region, $\mathbf{M}$, and the trained G and D, our goal is to get a restored image, $\hat{\mathbf{x}}$, close to the original image, $\mathbf{x}$. As a first step, the point, $\hat{\mathbf{z}}$, is found in the latent space corresponding to the given image as

$$\hat{\mathbf{z}} = \arg\min_{\mathbf{z}} (L_{contextual} + \lambda L_{perceptual}), \quad (2)$$

where λ is a weighting parameter, and

$$L_{contextual}(\mathbf{z}) = \|\mathbf{M} \odot (G(\mathbf{z}) - \mathbf{y})\|_1, \quad (3)$$

and

$$L_{perceptual}(\mathbf{z}) = \log(1 - D(G(\mathbf{z}))), \quad (4)$$

where $\odot$ is the Hadamard product operation.

Once $\hat{\mathbf{z}}$ is obtained, the image is completed as

$$\hat{\mathbf{x}} = \mathbf{M} \odot \mathbf{y} + (\mathbf{1} - \mathbf{M}) \odot \mathbf{G}(\hat{\mathbf{z}}), \quad (5)$$

where $\mathbf{1}$ denotes a matrix with elements equal to 1, so that $(\mathbf{1} - \mathbf{M})$ indicates the corrupted region.

3. SINOGRAM COMPLETION

3.1. Continuity Loss Function

The method described in Section 2.2 is able to find a point in the latent space based on the partial image and fill in the corrupted area with realistic content. Although the overall patterns of the filled-in region match those of the surrounding known region, the method does not produce a smooth border between them. The resulting image has discontinuities on the border of the two areas, thus requiring post-processing for blending the border region [15].

(a) (b)

Fig. 2: Masks for the contextual and continuity losses. Gray and black colors denote 1 and 0, respectively. (a) Mask for the known part, $\mathbf{M}$, and (b) the boundary mask, $\mathbf{M}_b$

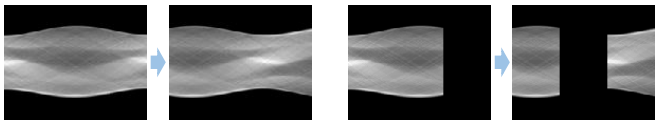

(a) (b)

Fig. 3: Rearrangement of the sinogram with circular shift (60° to the left) and vertical reflection. (a) 180° angle tomography, and (b) 120° angle tomography.

Clearly, the information near the border is more important than the remaining area for better estimation of the corrupted region. Therefore, we propose to add an additional loss term to place more weight on the border area and thus ensure consistency of the information near the boundary. We refer to it as *continuity loss* and define it as

$$L_{continuity}(\mathbf{z}) = \|\mathbf{M}_b \odot (G(\mathbf{z}) - \mathbf{y})\|_2^2, \quad (6)$$

where $\mathbf{M}_b$ denotes a boundary mask. Figure 2 illustrates the boundary mask, $\mathbf{M}_b$, in comparison with $\mathbf{M}$. The thickness of the boundary region in $\mathbf{M}_b$ is chosen empirically.

The total loss is therefore the sum of three loss terms as

$$L_{total} = \lambda_1 L_{contextual} + \lambda_2 L_{continuity} + \lambda_3 L_{perceptual}, \quad (7)$$

where λ_1, λ_2, λ_3 are the weighting parameters for each loss term.

3.2. Two-Ends Method

In the LAT, the missing angle views are located outside the known part as shown in Figs. 1 (b) and (c). Extrapolation is therefore performed to compensate for the missing information. However, we can convert the extrapolation task into an interpolation one by using a unique property of sinograms. In tomography, the projection at the angular distance of 180° means the projection along the exact opposite direction, but in reverse order. Thus, the projection at angle d° is identical to the vertically reflected projection at angle $(d + 180)^\circ$. This property allows a circular shift of sinogram by any degree without introducing any discontinuity inside the image as shown in Fig. 3 (a). By using this property, it is possible to rearrange the sinogram image so that both ends of the missing area of the sinogram touch known part of the sinogram.

Figure 3 (b) illustrates the rearrangement process of a sinogram of LAT. The missing area moves to the middle of the image from the right side, thus increasing the surrounding information for the missing region. After the image completion, we shift and flip the sinogram back to its original position.

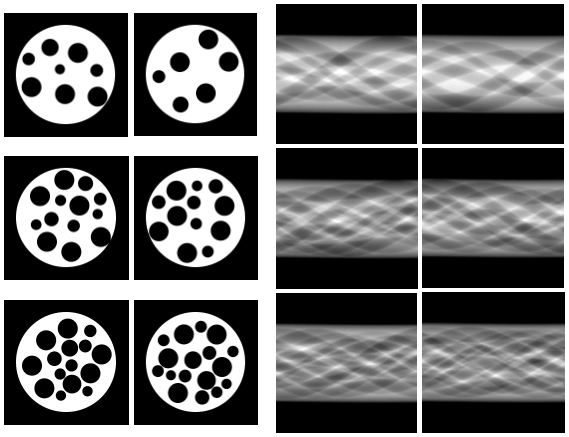

(a) (b)

Fig. 4: Examples of training dataset. (a) Phantoms, and (b) corresponding sinograms.

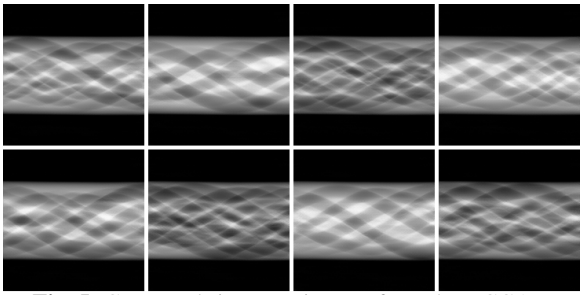

Fig. 5: Generated sinogram images from the DCGAN

4. EXPERIMENTAL RESULTS

4.1. DCGAN Training

For our experiments, we used *foam* type phantom images, which can be generated by a python software package, XDesign [18], as shown in Fig. 4 (a). The range of the pore size, gap between pores, and porosity are set to create different shapes of foams in a parameterized random manner. We converted them to the sinogram images by using the Radon transform, as shown in Fig. 4 (b). The sinograms were obtained for 180° angle tomography with 1° angular increment. The sizes of the phantom and the sinogram were 128×128 and 180×180, respectively. 9,000 singoram images were used for training.

We adopted the DCGAN architecture of [15] and changed the size of the layers and the number of the feature maps. The input for the generator, $\mathbf{z}$, is a 100-dimensional vector, whose elements are drawn with a uniform distribution from $[-1, 1]$. The generator has one fully connected layer for the first layer, and a series of deconvolutional layers with stride 2, doubling the image size at each layer. It outputs a one-channel image of size 192×192. The output image is larger than the size of the sinogram so it was cropped to obtain the final image. The architecture of the discriminator is the reverse of that of the generator except that it has an output of a scalar value instead of a 100-dimensional vector.

Stochastic gradient descent with the Adam optimizer [19] is used to train the DCGAN. We set the learning rate to 0.0001, the parameters, $\beta_1 = 0.5$, $\beta_2 = 0.999$, and the batch size to 64. Figure 5 shows the output of the trained DCGAN from 8 randomly chosen input vectors. The generated images look natural as real sinogram images although they produce non-natural phantoms when converted into the image domain.

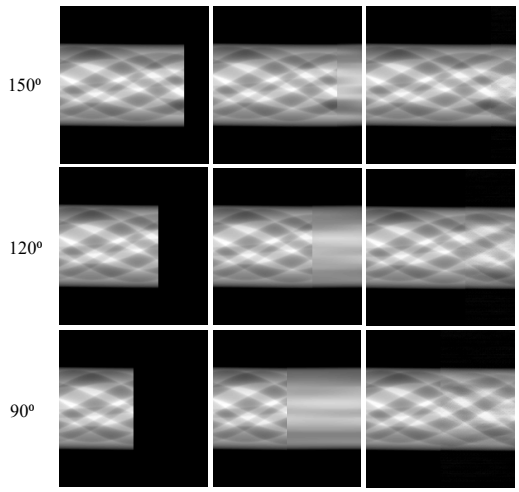

(a) (b) (c)

Fig. 6: Sinogram image completion for a test image from limited angle tomography with different angle views, 150°, 120°, and 90°. (a) LAT, (b) GPE, and (c) the proposed method

4.2. Experiments with Synthetic Data

The result of sinogram image completion for a test image is illustrated in Fig. 6. As shown in Fig. 6 (b), Gerchberg–Papoulis extrapolation (GPE) is not able to handle the complicated sinogram pattern. In contrast, in Fig. 6 (c), the proposed method generates the missing pattern seamlessly. Even with large amount of missing information (60°, 90°), the recovered sinogram looks quite natural. Note that we tuned the parameters for the sinogram extrapolation methods. For GPE, the cutoff frequencies are tuned with exhaustive search. The weighting parameters, λ_1, λ_2, and λ_3, in Eq. 5 are tuned for each image for our method. The weight for the perceptual loss, λ_3, is set to a small value (0.1). The performance of the image completion is not sensitive to the value of λ_3. λ_1 and λ_2 are set to 0 and 1, respectively, for 30° of the missing angle, and both to 1, otherwise. It reflects the fact that the information near the border is enough for small missing data, but more data is needed with large missing data.

We also see in Fig. 7 that the proposed method suppresses the artifacts effectively in the image domain. It is compared with two other approaches: (1) FBP reconstruction without any extrapolation (LAT), and (2) FBP reconstruction with GPE [11]. The reconstruction from LAT shows elongation artifacts and two streaks from the edges. Those artifacts become extremely severe when the missing angle is 90°. Both GPE and the proposed method effectively suppress the artifact outside the object. However, the reconstruction from GPE still contains severe elongation and blurring artifacts inside the phantom. Since the proposed method restores the sinogram better, it results in fewer artifacts and better contrast of the image.

The performance of reconstruction is summarized in Table 1. PSNRs and SSIMs are calculated from the reconstruction of 4 test images and the average numbers are recorded. Note that these metrics are calculated in the image domain, not in the sinogram domain, because our ultimate goal is a better reconstruction in the image domain. The PSNRs achieved by the proposed method are significantly higher than those by other methods, about 7 dB higher than those of LAT and up to 3 dB higher than those of GPE.

The proposed method has robustness to noise as shown in Fig. 8 and Table 2. To simulate the noisy measurements, we added Gaussian noise to the sinograms with two different standard deviations: $\sigma_n = 0.01$ and $\sigma_n = 0.05$. The results show that, even with noise,

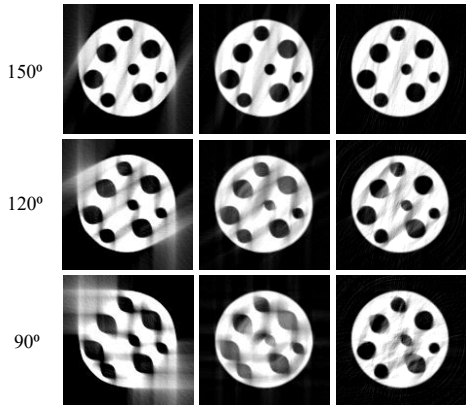

Fig. 7: FBP reconstruction for a test image from limited angle tomography with different angle views, 150°, 120°, and 90°. (a) LAT, (b) GPE, and (c) the proposed method

Table 1: Performance of reconstruction

Missing angles	30°		60°		90°	
Method	PSNR	SSIM	PSNR	SSIM	PSNR	SSIM
LAT	15.52	0.2804	10.75	0.1982	7.35	0.1401
GPE	18.45	0.4866	15.28	0.4183	13.58	0.3810
Proposed	**21.66**	**0.5965**	**17.41**	**0.4472**	**15.14**	**0.3783**

Table 2: Performance of reconstruction from noisy data

Missing angles		30°		60°		90°	
σ_n	Method	PSNR	SSIM	PSNR	SSIM	PSNR	SSIM
0.01	LAT	15.22	0.2493	10.64	0.1815	7.30	0.1293
	Proposed	**20.72**	**0.4380**	**16.98**	**0.3777**	**14.55**	**0.3369**
0.05	LAT	10.92	0.1542	8.30	0.1138	5.76	0.0801
	Proposed	**13.47**	**0.2085**	**13.03**	**0.1980**	**12.44**	**0.1872**

the proposed method is able to estimate the missing patterns effectively. Note that it generates noiseless sinogram patterns although the input sinogram is noisy. It is because the DCGAN is trained with noiseless sinogram images.

4.3. Experiments with Real Data

To validate the proposed method, we tested it with experimental data from a $LiNi_{0.8}Co_{0.15}Al_{0.05}O_2$ cathode in a fully-assembled in-situ lithium-ion tomography cell, which allows X-ray transmission over 150° of rotation. Full-field transmission X-ray microscopy was performed at sector 32-ID-C of the Advanced Photon Source [20]. Again, we used XDesign [18] to generate the training images that are consistent with the given data. 9,000 sinogram images are used

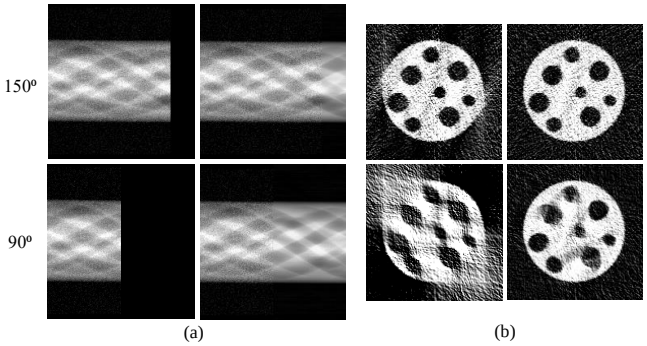

Fig. 8: Experimental results with the noisy data ($\sigma_n = 0.05$). The top and bottom rows are the cases of 150° and 90° angle tomorgraphy, respectively. (a) Signoram completion, and (b) FBP reconstruction from (a).

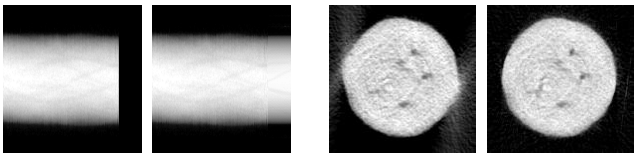

Fig. 9: Sinogram image completion and image reconstruction with an experimental data. (a) Sinogram image completion, and (b) FBP image reconstruction from (a).

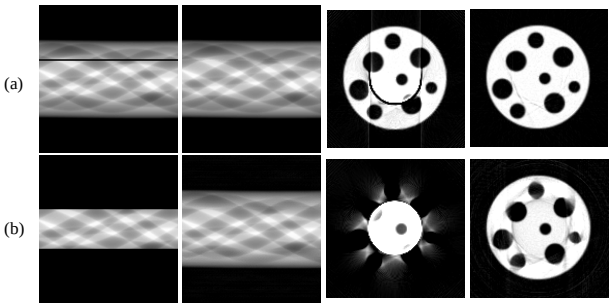

Fig. 10: Other applications. The first and second columns show sinograms with missing information, and the restored sinogram. The third and fourth columns show the image reconstruction from sinograms in the first and second columns, respectively. (a) Ring artifact removal in tomography, and (b) truncated tomography.

to train a DCGAN for the real data. Figure 9 shows sinogram image completion and image reconstruction from the real data. The real data is more challenging due to more noisy and blurry patterns and non-uniform intensity of the projections. Nevertheless, the proposed method recovers missing pattern and improves the image reconstruction.

4.4. Other Applications

We present two other applications to show that our method can solve a broad range of problems. The first application is a ring artifact removal problem in tomography [21,22]. Defective elements in the detector cause stripes in the sinogram, resulting in a ring artifact in its tomographic reconstruction. With the proposed method, the missing information is restored and thus the ring artifact is removed as shown in Fig. 10 (a). The second one is truncated tomography [23, 24]. When the object is larger than the field of view (FOV) of the detector, the information outside the FOV is cut off. Then the upper and lower parts of the sinogram get truncated. The missing information of the truncated tomography can be also recovered by the proposed method as shown in Fig. 10 (b). The proposed method works effectively even though a large amount of information is missing outside of the FOV.

5. CONCLUSION

In this paper, we have presented a novel extrapolation-based method to tackle the LAT problem. We train a DCGAN to generate sinograms and use it to perform sinogram image completion. Incorporation of the continuity loss and the two-ends scheme enables the method to find the missing patterns of sinograms, and results in better sinogram completion and image reconstruction. Experimental results show the effectiveness of the proposed method both with respect to objective measures and visual quality. It is also shown that the method can be extended to solve other tomography problems with missing information.

6. REFERENCES

[1] C. Tomasi and R. Manduchi, "Bilateral filtering for gray and color images," in *Proceedings of the Sixth International Conference on Computer Vision*, Washington, DC, USA, 1998, ICCV '98, pp. 839–, IEEE Computer Society.

[2] A. S. Frangakis and R. Hegerl, "Noise Reduction in Electron Tomographic Reconstructions Using Nonlinear Anisotropic Diffusion," *Journal of Structural Biology*, vol. 135, no. 3, pp. 239–250, sep 2001.

[3] H. Zhang, L. Li, K. Qiao, L. Wang, B. Yan, L. Li, and G. Hu, "Image Prediction for Limited-angle Tomography via Deep Learning with Convolutional Neural Network," *arXiv*, 2016.

[4] J. Frikel, "Sparse regularization in limited angle tomography," *Appl. Comput. Harmon. Anal*, vol. 34, pp. 117–141, 2013.

[5] B. Goris, W. Van den Broek, K.J. Batenburg, H. Heidari Mezerji, and S. Bals, "Electron tomography based on a total variation minimization reconstruction technique," *Ultramicroscopy*, vol. 113, pp. 120–130, feb 2012.

[6] Z. Chen, X. Jin, L. Li, and G. Wang, "A limited-angle CT reconstruction method based on anisotropic TV minimization," *Physics in Medicine and Biology*, vol. 58, no. 7, pp. 2119–2141, apr 2013.

[7] Y. Huang, O. Taubmann, X. Huang, V Haase, G. Lauritsch, and A. Maier, "A new weighted anisotropic total variation algorithm for limited angle tomography," in *2016 IEEE 13th International Symposium on Biomedical Imaging (ISBI)*. apr 2016, pp. 585–588, IEEE.

[8] S. F. Yau and S H. Wong, "A linear sinogram extrapolator for limited angle tomography," in *Proceedings of the International Conference on Signal Processing*. 1996, vol. 1, pp. 386–389, IEEE.

[9] A. P. Happonen and U. Ruotsalainen, "A Comparative Study of Angular Extrapolation in Sinogram and Stackgram Domains for Limited Angle Tomography," in *Image Analysis*, pp. 1047–1056. Springer, Berlin, Heidelberg, 2005.

[10] Y. Huang, X. Huang, O. Taubmann, Y. Xia, V. Haase, J. Hornegger, G. Lauritsch, and A. Maier, "Restoration of missing data in limited angle tomography based on HelgasonLudwig consistency conditions," *Biomedical Phys. Eng. Express*, vol. 3, 2017.

[11] A. Papoulis, "A new algorithm in spectral analysis and bandlimited extrapolation," *IEEE Transactions on Circuits and Systems*, vol. 22, no. 9, pp. 735–742, sep 1975.

[12] A. Van Den Oord, N. Kalchbrenner, and K. Kavukcuoglu, "Pixel Recurrent Neural Networks," *ICML*, 2016.

[13] D. Pathak, P. Krahenbuhl, J. Donahue, T. Darrell, and A. A. Efros, "Context Encoders: Feature Learning by Inpainting," *CVPR*, 2016.

[14] R. Gao and K. Grauman, "From One-Trick Ponies to All-Rounders: On-Demand Learning for Image Restoration," *arXiv*, 2017.

[15] R. Yeh, C. Chen, T. Y. Lim, M. Hasegawa-johnson, and M. N. Do, "Semantic Image Inpainting with Perceptual and Contextual Losses," *arXiv:1607.07539v2*, 2016.

[16] I. Goodfellow, J. Pouget-Abadie, and M. Mirza, "Generative Adversarial Networks," *arXiv*, pp. 1–9, 2014.

[17] A. Radford, L. Metz, and S. Chintala, "Unsupervised Representation Learning with Deep Convolutional Generative Adversarial Networks," *arXiv*, pp. 1–15, 2015.

[18] D. J. Ching and D. Gürsoy, "XDesign: an open-source software package for designing X-ray imaging phantoms and experiments," *Journal of Synchrotron Radiation*, vol. 24, pp. 537–544, 2017.

[19] D. P. Kingma and J. Ba, "Adam: A Method for Stochastic Optimization," dec 2014.

[20] V. De Andrade, A. Deriy, M. Wojcik, D. Gürsoy, Shu K. Fezzaa, and F. De Carlo, "Nanoscale 3D imaging at the Advanced Photon Source," *SPIE Newsroom*, pp. 2–4, May 2016.

[21] M. Boin and A. Haibel, "Compensation of ring artefacts in synchrotron tomographic images," *Optics Express*, vol. 14, no. 25, pp. 12071, dec 2006.

[22] B. Münch, P. Trtik, F. Marone, and M. Stampanoni, "Stripe and ring artifact removal with combined waveletFourier filtering," *Optics Express*, vol. 17, no. 10, pp. 8567, may 2009.

[23] J. Hsieh, E. Chao, J. Thibault, B. Grekowicz, A. Horst, S. McOlash, and T. J. Myers, "A novel reconstruction algorithm to extend the CT scan field-of-view," *Medical Physics*, vol. 31, no. 9, pp. 2385–2391, aug 2004.

[24] Y. Xia, M. Berger, S. Bauer, S. Hu, A. Aichert, and A. Maier, "An Improved Extrapolation Scheme for Truncated CT Data Using 2D Fourier-Based Helgason-Ludwig Consistency Conditions," *International Journal of Biomedical Imaging*, pp. 1–14, jul 2017.